

# Multipoint Variable parameter compliant control of redundant manipulator based on the equivalent twin model of flexible contact dynamics

*International Journal of Advanced  
Robotic Systems*  
September–October 2024: 1–16  
© The Author(s) 2024  
Article reuse guidelines:  
sagepub.com/journals-permissions  
DOI: 10.1177/17298806241283702  
journals.sagepub.com/home/axr



Genliang Xiong<sup>1</sup>, Lan Ye<sup>2</sup>, Xiaoqing Zhang<sup>1</sup> , Yanfeng Gao<sup>1</sup>,  
Zhang Hua<sup>1</sup>, Yang Dapeng<sup>3</sup>, Chao Yu<sup>4</sup> and Qirong Tang<sup>5</sup>

## Abstract

To elucidate the dynamic coupling mechanism involved in multipoint/arbitrary point contact during human–robot interactions with redundant manipulators, we introduce a compliant control strategy that adapts to variable parameters. This strategy is based on the flexible contact dynamic equivalent twin system for human–robot interactions. Using the Virtual Elastic Element Representation model for arbitrary point contact dynamics and leveraging the skeleton principle for contact force conversion, we construct a flexible contact dynamic equivalent twin system tailored for redundant manipulators with multipoint/arbitrary point contact capabilities. Within this system, we implement real-time adjustments to the impedance stiffness coefficient in conjunction with the virtual end velocity of the manipulator. We optimize the joint angular velocity of the manipulator while considering the motion allocation of redundant degrees of freedom. This optimization enables multipoint contact variable parameter compliance control for safe human–robot interactions. To validate our approach, we analyze the multipoint contact dynamic model of the redundant manipulator’s interaction with humans and assess the feasibility of the variable parameter compliance control method using robot operating system simulations. Ultimately, we verify the effectiveness and practicality of our proposed compliance control method through simulation and experimental results.

## Keywords

Variable impedance control, VEER, redundant manipulator, multipoint contact, human–robot interaction

Date received: 24 November 2023; accepted: 20 August 2024

Topic: AI in Robotics; Human Robot/Machine Interaction

Topic Editor: Alessandro Di Nuovo

Associate Editor: Ankita Rajput

## Introduction

Unlike nonredundant robots, redundant manipulators feature more degrees of freedom than strictly required to perform a specific end-effector task. This surplus of degrees of freedom enables them to undertake additional tasks, such as joint limit avoidance,<sup>1</sup> obstacle avoidance,<sup>2–4</sup> and singularity avoidance,<sup>5,6</sup> thereby optimizing robot motion. Consequently, redundant manipulators find widespread applications in fields demanding higher precision, efficiency, flexibility, and robustness, particularly in

<sup>1</sup> School of Mechanical and Automotive Engineering, Shanghai University of Engineering Science, Shanghai, China

<sup>2</sup> School of Advanced Manufacturing, Nanchang University, Nanchang, China

<sup>3</sup> State Key Laboratory of Robotics and System, Harbin Institute of Technology, Heilongjiang, China

<sup>4</sup> R&D Department, Shanghai Junctrl Robot Co., Ltd. 401, Shanghai, China

<sup>5</sup> The Laboratory of Robotics and Multibody System, School of Mechanical Engineering, Tongji University, Shanghai, China

### Corresponding author:

Genliang Xiong, School of Mechanical and Automotive Engineering, Shanghai University of Engineering Science, Shanghai 201620, China.

Email: xiongenliang7865@163.com

Data Availability Statement included at the end of the article



unstructured environments. In various operational scenarios, including human–robot interaction, rehabilitation care, human body massage, subcutaneous injections, and flexible object grasping, the dual control of both the position and force of the manipulator becomes imperative. In unstructured environments, different objects typically exhibit distinct mechanical characteristics. These adjustments maintain the technical content while enhancing the overall flow and readability of the paragraph.

Even within the same object, mechanical properties can vary across different regions due to biological signals, tissue structures, and various factors. This uncertainty in material types and their mechanical characteristics can result in significant tracking errors or even the loss of force tracking capability when employing traditional impedance control methods. Additionally, much of the existing literature on human–robot interaction control typically assumes that interactions occur at a single point, often at the manipulator’s end-effector. However, this doesn’t hold true in many social scenarios. For instance, when a nursing robot lifts a patient or a humanoid robot engages in a hug with a human, as depicted in Figure 1, interactions occur not only at one single point but also at multiple points, assuming that a contact area can be approximated as a single point. Achieving compliant control for multipoint human–robot interactions poses a significant challenge. To address the limitations of traditional impedance control methods for redundant manipulators, including their limited adaptability, poor robustness, challenges in parameter tuning, insufficient flexibility in handling interactions, sensitivity to model errors, and their inability to support multipoint interactions, this paper focuses on researching variable-parameter compliant control for redundant manipulators. Our approach is grounded in the study of contact dynamics in human–robot interactions.

To ensure the safe and user-friendly operation of redundant manipulators during interactions with humans in unstructured environments, several approaches can be taken. In addition to optimizing mechanical designs and enhancing collision detection with supplementary sensors, maintaining the manipulator’s configuration similarity during motion is primarily achieved through planning redundant degrees of freedom. Furthermore, achieving similarity in response after contact is primarily accomplished through manipulator compliance control. Robot compliance control methods generally fall into two categories: passive compliance control and active compliance control.<sup>7</sup> Passive compliance control involves the installation of compliant devices on the robot’s body to achieve the desired compliant behavior. In contrast, active compliance control establishes control models to enable compliant operations. Active compliance control includes two main approaches: impedance control<sup>8</sup> and force/position hybrid control.<sup>9,10</sup>

Hybrid force/position control involves decomposing force and position into orthogonal subspaces, typically under specific conditions. Zhang et al.<sup>11</sup> introduced an improved approach building upon force/position hybrid control. In their method, they replace the position loop in the operating space with an equivalent joint position loop. Subsequently, the Jacobian matrix is calculated based on the actual robot parameters to achieve force control. However, pure force/position control may exhibit limitations. It often needs to switch between force and position control modes, which can result in reduced robustness and a strong reliance on the environment. To enhance system robustness against external interference, Song<sup>12</sup> incorporated a smooth robust compensator into the robot’s force control system, leading to a notable improvement in system’s antiinterference capabilities. Dong et al.<sup>13,14</sup> took

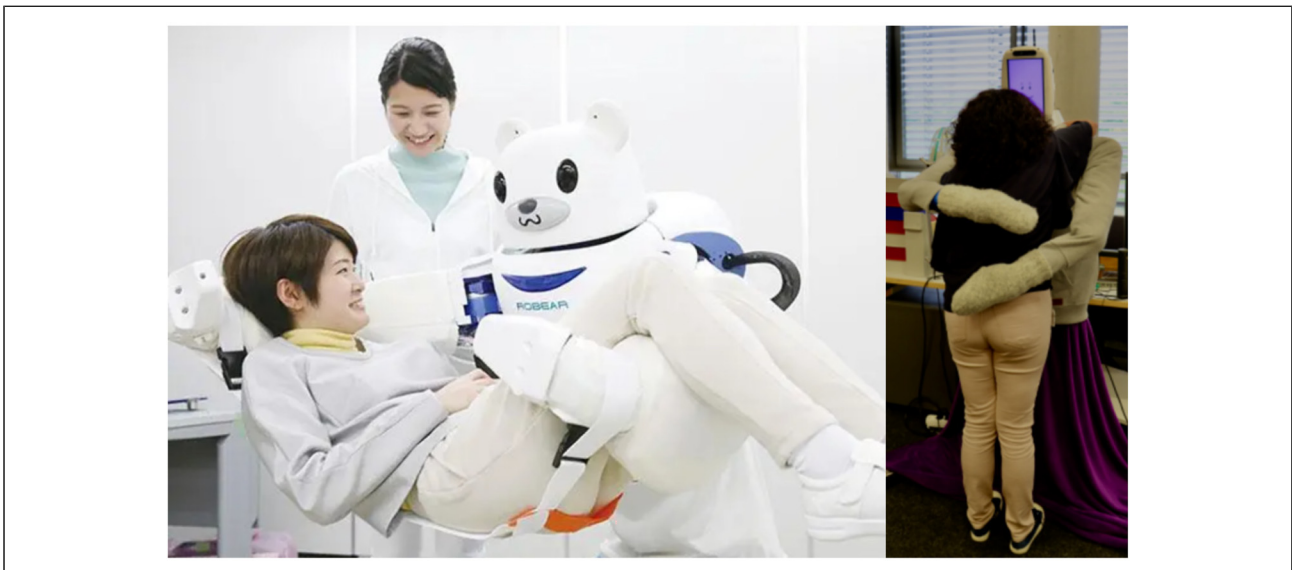


Figure 1. Human–robot interaction.

a different approach by applying the principles of sliding mode control to end force control in robots. This approach offers the advantage of global asymptotic stability even when dealing with bounded disturbances. Recognizing this advantage, Xiang<sup>15</sup> introduced an adaptive algorithm into the force/position hybrid control of the robot. This allowed them to employ sliding mode control to eliminate dead zone parameter errors, thereby ensuring the accuracy and robustness of both position and force control.

The precise control of forces in robots through impedance control has been a significant focus for researchers worldwide. In the early 1980s, Hogan<sup>16</sup> made a pioneering contribution by suggesting that the interaction between a manipulator and its environment could be viewed as an impedance and admittance system. He proposed that compliance during interaction could be adjusted by considering the dynamic relationship between the manipulator's end and the contact force. This perspective offered a solution to the contact problem from an energy standpoint. The primary challenge in impedance control lies in tuning the robot's impedance parameters. Traditional methods involve using constant impedance parameters,<sup>17</sup> which can lead to performance limitations, especially when robots collaborate with humans or operate in unstructured environments. To address this limitation, researchers have introduced impedance control methods with variable parameters.<sup>18</sup> These methods reduce the need for precise mathematical modeling of both the robot and its environment. Seraji et al.<sup>19</sup> developed an adaptive impedance control scheme, which partially compensates for uncertainties in environmental factors while remaining simple and efficient to implement. Lu<sup>20</sup> introduced the Lyapunov equation within impedance control, demonstrating improved adaptability to uncertain parameters in force control processes. Ikeura and Tsumugiwa<sup>21,22</sup> independently modified the damping value of impedance control online based on force minimization and measured the stiffness change of the human arm online, achieving variable adjustments to impedance parameters. Sharifi et al.<sup>23</sup> proposed a nonlinear model reference adaptive impedance controller to achieve compliance in human-robot interaction. They applied this method to a two-degree-of-freedom robot with an end-effector moving in the  $x$ - $z$  plane for simulation analysis. However, this approach, based on Lagrange's dynamic equations for two degrees of freedom, may lack generality due to its relative simplicity. These studies have made significant strides in achieving variable-parameter end compliance control through analyses of manipulation tasks and human movements. Yet, despite their advancements, these studies often neglect the robot's motion configuration throughout human-robot interaction, limiting their ability to handle complex operational tasks in unstructured environments.

To address the control challenges faced by robots operating in unstructured environments, researchers have introduced a control approach that simultaneously manages both

the redundant degrees of freedom and the compliance performance of manipulators. In specific scenarios, Peng et al.<sup>24</sup> achieved motion control for redundant manipulators while optimizing their redundant degrees of freedom based on task-specific objective functions. Ficuciello et al.<sup>25</sup> made a groundbreaking contribution by combining variable parameter impedance control with solutions for redundant degrees of freedom, resulting in enhanced stability during human-robot interactions. They accomplished this by adjusting the impedance parameters of redundant manipulators in Cartesian space. For flexible joint redundant manipulators engaged in physical human-robot interaction, Xiong et al.<sup>26</sup> proposed and verified an adaptive dynamic method based on virtual decomposition Cartesian impedance control. This method offers effective adaptability. Li<sup>27</sup> introduced a robot controller equipped with feed-forward force and impedance adaptive compensation for interactions with the environment, contributing to improved performance. Peng et al.<sup>28</sup> addressed specific user objectives by designing two redundant manipulator compliant motion controllers and introducing additional constraints through redundant degrees of freedom. Furthermore, the literature has explored compliant operation in redundant manipulators by augmenting the operating space, incorporating augmented kinematics, and employing impedance control methods.<sup>29,30</sup> In addition, in order to improve the flexibility and efficiency of this paper's method for redundant manipulators in multi-touch environments, the literature<sup>31,32</sup> method is a good reference.

In summary, the dynamic coupling mechanism during contact interactions between redundant manipulator systems and humans in multipoint contact positions remains unclear. While some scholars have proposed collision detection algorithms that can determine the robot's collision position and the direction of collision forces using sensors, this approach often involves the addition of costly force sensors, which may hinder the widespread adoption of collaborative manipulators. As a result, there is currently no effective strategy to address contact occurring at various points along the links of redundant manipulators, particularly in scenarios involving multipoint contact with compliant behavior. To address this gap in knowledge, this manuscript delves into the study of multipoint variable parameter compliant control for redundant manipulators, leveraging the concept of an equivalent twin model of flexible contact dynamics.

## **Construction of equivalent twin system for flexible contact dynamics**

### *Dynamic model of arbitrary point contact based on virtual elastic element representation*

It is a well-known fact that if a robot system is entirely rigid, collisions will result in instantaneous impacts. However,

real robotic systems are designed to maintain contact with humans or objects for a certain period before a collision is deemed likely. Moreover, during contact, the point of contact can occur anywhere along the robot's structure (see Figure 2). To effectively calculate the contact force at the collision point, this section introduces a description of the robot structure represented by a virtual elastic element, referred to as Virtual Elastic Element Representation (VEER). In this representation, the contact part is equivalently modeled as the buffering effect of a spring-damper system, as depicted in Figure 2(a). Using this structure, we can construct the dynamic model of the manipulator for contact at any point.

As shown in Figure 2(b), the virtual elastic element comprises two distinct regions: a rigid area within the base and an elastic area within the working space reachable by the mechanical arm. The rigid region is centrally positioned within the frame, surrounded by the elastic region. It's important to emphasize that the base of the manipulator must remain entirely within the rigid area to ensure that the manipulator and base remain in contact without deformation. When a person or the environment comes into contact with the manipulator, they interact with the elastic area. The force experienced depends on the elasticity level and the extent of distance change resulting from the contact.

For the case of arbitrary point contact with the manipulator, we apply Hertz theory to solve contact mechanics problems within the VEER framework, combined with reference.<sup>34</sup> Several simplified assumptions are as follows:

1. The body is assumed to be homogeneous, isotropic, and linearly elastic, with plastic flow treated quasi-statically.
2. Contact occurs between objects with nonconformal geometry, where the contact area is smaller than the size of the colliding objects, and is considered independent of most of the stress in the two objects.
3. For compliant point contact, we assume that the contact area is very small, and the magnitude of the contact

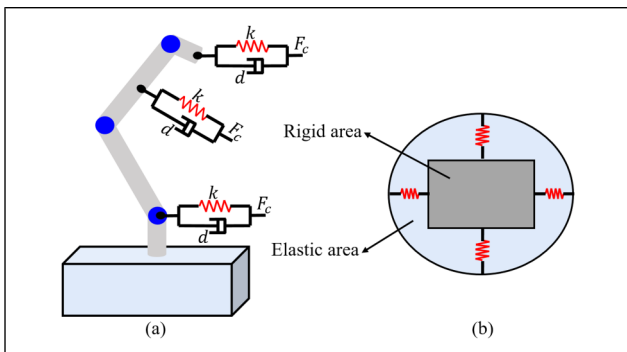


**Figure 2.** VEER structure description (a) state diagram of human-robot contact part (b) representation diagram of virtual elastic element.

VEER: Virtual Elastic Element Representation.

force is much smaller than that during the impact. Consequently, the manipulator's speed is slow at the moment of contact, and the speed remains constant before and after the collision.

For two objects  $i$  and  $j$  in point contact, the flexible contact model based on Hertz theory<sup>33</sup> is shown in Figure 3 on the premise of satisfying the assumption condition (2). Assume that the object  $j$  that is about to come into contact with any point of a segment  $i$  of the manipulator, and the two object coordinate systems are denoted by  $K_i$  and  $K_j$ , respectively. The origin of each coordinate system is located by the position vectors  $r_i$  and  $r_j$  with respect to the world coordinate system  $K_w$ , and its translation and rotation transformations are denoted by  $B_i$ ,  $B_j$ ,  $R_i$ , and  $R_j$ , respectively. Since the link of the manipulator is a cylinder, according to the assumption (2), the point contact between the manipulator and the object can be equivalent to the contact between a sphere and a plane, as shown in Figure 3(b). At this time, the position of the center of the sphere  $A$  relative to  $K_i$  is  $r_A$ , and the sphere radius is  $R$ . The action point  $p_a$  is defined as the contact point of two objects at the moment of contact. After the flexible contact occurs, the surface of the plane  $B$  is located at a height  $h_j$  along the plane normal  $n$  from the origin of the coordinate system  $K_j$ .

Hertz theory typically describes the flexible contact model by relating the penetration depth of two objects to the contact force. The local deformation can be parameterized as a function of the undeformed penetration depth. As a result, the compliant normal contact force model during contact can be equated to a nonlinear spring-damper model,<sup>34</sup> expressed as:

$$f_n = \lambda|x|^p\dot{x} + k|x|^p \quad (1)$$

where  $|x|$  is the maximum distance of relative penetration of two objects,  $\dot{x}$  is the speed of the contact point. When two objects are in point contact, we know that  $p=3/2$  based on Hertz's theory. The stiffness coefficient  $K$  is related to the geometry of the contact body and the Young's

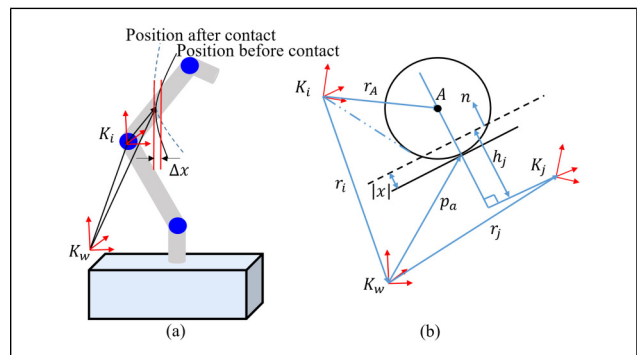


**Figure 3.** Point contact model based on hertz theory. (a) Human-robot arbitrary contact model diagram. (b) Equivalent model diagram of arbitrary contact.

modulus of the material. When the manipulator contacts a person, the contact force model resembles that of a spherical surface and a plane, and we can calculate the stiffness coefficient  $K$  using the following equation:

$$k = \frac{4}{3\pi(h_{m,i} + h_{m,j})} R_i^{1/2} \quad (2)$$

where  $h_{m,i}$  and  $h_{m,j}$  represents the material properties of the sphere  $i$  and the plane  $j$ , respectively, whose values depend on the Poisson's ratio  $\nu_n$  and Young's modulus  $E_n$  of each object

$$h_{m,n} = \frac{1 - \nu_n^2}{\pi E_n}; n = i, j \quad (3)$$

$\lambda$  is the hysteresis damping coefficient. Assuming that the energy dissipation is symmetrically distributed around the hysteresis loop, the hysteresis damping coefficient is calculated as following:

$$\lambda = \frac{3}{4}(1 - e_{emp}^2) \frac{1}{\pi v_r} k; e_{emp} = 1 - \alpha v_r \quad (4)$$

where  $\alpha$  is an empirical value that depends on the impact speed within a limited range,  $v_r$  is the relative velocity of the two bodies at the initial moment of contact.

To sum up, based on the VEER architecture and Hertz theory, the flexible contact dynamics model of any point during the human-robot interaction process can be derived, which is essentially a nonlinear spring, used to estimate the interaction force of two objects in contact and collision, this lays the foundation for the subsequent development of compliance control. It should be noted that the model is based on the premise that two objects collide at low speed, so it must be implemented in small steps in the simulation.

### Skeleton-based equivalent transformation of point contact force

For the serial manipulator, the force generated by the end contact will be transmitted through the shoulder, elbow, and wrist joints of the manipulator. This implies that the force resulting from contact at any point on the manipulator will ultimately affect its joints. Building upon the VEER flexible dynamic model of arbitrary point contact introduced in the dynamic model of arbitrary point contact based on virtual elastic element representation section, this section will delve into the description of contact force transformation using a skeleton model.

In the case of a manipulator with multiple degrees of freedom, the final position of its end-effector relies on the motion of its links influenced by the joints. To manage this complexity, we divide the serial redundant manipulator into two key segments: moving segment ( $MS$ ), representing the manipulator's body, and joint segment ( $JS$ ), representing the joints. By integrating the Denavit-Hartenberg

(D-H) parameter description of the manipulator, we can treat the manipulator as a skeleton control node with position joints. The segments, represented by  $MS$ , are created by connecting lines between these nodes, thus constructing a skeleton model of the manipulator, as illustrated in Figure 4(a). In the order from the base to the manipulator's endpoint, the other  $MS$ s/ $JS$ s are referred to as  $MS_1$ ,  $JS_1$ ,  $MS_2$ ,  $JS_2$ , ...  $MS_{n-1}$ ,  $JS_{n-1}$ ,  $MS_n$ , respectively. For the shoulder joint, because the base is fixed, the shoulder joint is fixed, so the selection of skeleton nodes starts from the elbow joint, that is control point ( $CP$ ) ( $CP_1$ ,  $CP_2$ , and  $CP_3$ ) in the figure. We can place any control points wherever on the manipulator as can be seen Figure 4. We place the  $i$ th control point ( $CP_i$ ) on the center of the  $JS_i$ . In the case of  $i=n$ , we place the  $n$ th control points ( $CP_n$ ) on the tip of the  $MS_n$  so that the  $CP_n$  coincide with the manipulator's endpoint. By placing the control points in this way, at least two degrees of freedom are used to decide one control point's position.

The equivalent force contact model, based on the skeleton, is derived from the segmented skeleton of the 7-DOF redundant manipulator, comprising shoulder, elbow, and wrist joints, as depicted in Figure 4(b). Using the motion resulting from the force at the contact points, we can convert the contact force generated at each elastic element into an equivalent force applied to the control node of the manipulator. This conversion is based on the VEER concept, combined with the virtual end described in.<sup>35</sup> Through dynamic simulation, we observe that the effect of force transmission to the base of the manipulator is notably pronounced. Therefore, in Figure 4(b), when a contact occurs at a position where the distance of the control node  $CP_{i+1}$  of the manipulator is  $l_i$  and the magnitude of the contact force is  $f_i$ , the length between the two control nodes  $CP_{i+1}$  and  $CP_i$  of manipulator is  $L_i$ . The force  $F_i$  acting on the control node  $CP_i$  can be derived as:

$$F_i = \frac{l_i}{L_i} f_i \quad (5)$$

Combined with equation (1), the contact force at any position can be deduced  $f_i$ . Then, on the premise of obtaining

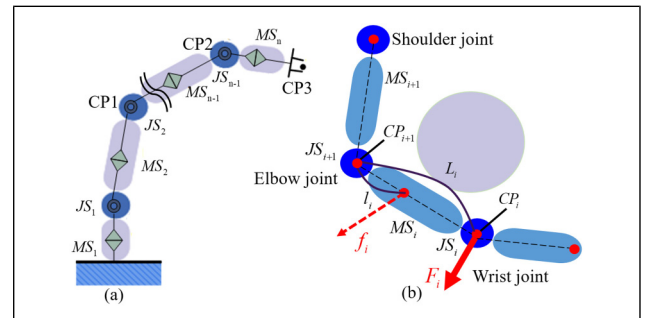


**Figure 4.** Skeleton-based contact force transformation. (a) Skeleton model of manipulator. (b) Skeleton-based equivalent force contact model.

the position information of the contact point, the force estimation value  $F_i$  equivalent to the corresponding joint control node can be obtained through equation (5).<sup>36</sup>

Because of the change of force on the joint, when there is an external force on any segment of the manipulator, the position of the manipulator will be offset, and the greater the external force applied, the greater the offset of the corresponding control point. In order to facilitate the implementation of the subsequent compliance control strategy, the force  $F_i$  on the position joint control node of the manipulator can be subjected to virtual end equivalence. Its implementation method needs to be obtained by means of force Jacobian equivalence, while the virtual end equivalent force Jacobian  $J_F$  and pseudo-inverse matrix  $J_F^+$  refer to.<sup>35</sup>

### Equivalent twin system description of flexible contact dynamics

When the manipulator is subjected to an external force at any position, especially at multiple points, the manipulator will produce joint acceleration, and then the end of the manipulator will accelerate in Cartesian space. In order to achieve the goal of compliance control, subject to Newton's second law, that is to say, the acceleration acting on the end of the manipulator is determined by the resultant external force, and its equivalent mass affects the generation of acceleration. In the context of human-robot interaction, if the forces acting on the manipulator under multipoint contact at any position can be equated to the force acting on the end of the manipulator, which includes the mass and inertia of all the manipulator's structures (as shown in Figure 5(a)), then the mass of the joints and links has minimal impact on the dynamics, often being negligible. Consequently, compliant behavior becomes more likely under the influence of contact forces, akin to an inverse kinematics effect of rotation around the end of the manipulator's axis (as depicted in Figure 5b)). In this representation, an oversized sphere symbolizes the mass

of the joints and links being equivalent to the end. Under these conditions, the links and joints can be treated as having negligible mass.

Our goal is to achieve  $H^{-1}(q)$  as an almost constant diagonal matrix, the problem of inverse dynamic selection of joint angular acceleration, angular velocity and joint angle is realized by adjusting the external force compliance, which is called the dynamic equivalent twin system in this paper. The calculation of  $H$  is as follows:

According to the forward kinematics, combined with the D-H parameters of the manipulator, the joint position  $q$  of the manipulator mapping relationship with the pose of the end of the manipulator in Cartesian space is expressed by the following equation:

$$x = g(q) \quad (6)$$

The inverse kinematics of the manipulator can be solved using  $q = g^{-1}(x)$  to express. The relationship between the joint velocity vector  $\dot{q}$  and the end velocity vector  $\dot{x}$  is transformed by means of an equivalent force Jacobian, which equivalent force Jacobian matrix can be calculated by  $J_F = WJ$ ,<sup>27</sup> then:

$$\dot{x} = J_F \dot{q} \quad (7)$$

Differentiate equation (7) with respect to time to obtain an expression for the end acceleration:

$$\ddot{x} = J_F \ddot{q} + \dot{J}_F \dot{q} \quad (8)$$

From the basic dynamics equation  $M_q(q)\ddot{q} + C_q(q, \dot{q})\dot{q} + G_q(q) = \tau$ , the angular acceleration driven by the moment at the end of the manipulator can be obtained as:

$$\ddot{q} = M_q^{-1} J_F^T F - M_q^{-1} C_q \dot{q} - M_q^{-1} G_q \quad (9)$$

$F$  is the force that drives the joint. Combined with the assumptions of Hertz theory, the relationship between instantaneous joint acceleration and driving force can be simplified by neglecting nonlinearity, velocity-related terms and gravity-induced acceleration as follows:

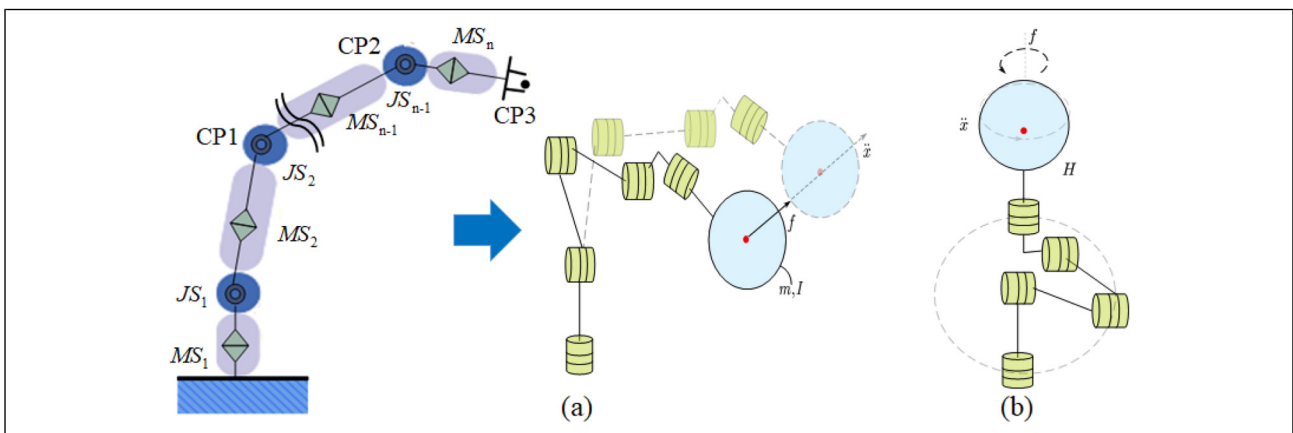


**Figure 5.** Manipulator dynamics equivalent twin system. (a) Manipulator end equivalent mass. (b) End equivalent motion.

$$\ddot{q} = M_q^{-1} J_F^T F \quad (10)$$

When the instantaneous speed of the manipulator is zero, it can be obtained from equations (8) and (10):

$$\ddot{x} = J_F M_q^{-1} J_F^T F \quad (11)$$

Combining equations (10) and (11), the inertia matrix  $M_q^{-1}$  of manipulator has a close influence on the generation of the acceleration  $\ddot{q}$  of the manipulator joint, and the position of the manipulator will be deviated under the drive of force. Therefore, it can be inferred that the acceleration of the manipulator joint is a reflection of the error vector of the in Cartesian space, so that the acceleration of the manipulator in the Cartesian space can be realized under the condition of the kinematic constraints, the direction of  $\ddot{x}$  depends on the direction of the force.

Based on above, the equivalent mass matrix defined in this subsection  $H^{-1} = J_F M_q^{-1} J_F^T$ , leading to a more concise representation:

$$\ddot{x} = H^{-1} F \quad (12)$$

## Design of compliant controller with variable parameters for multipoint contact

### General description of the algorithm

The multipoint contact variable parameter compliance control strategy, as presented in Figure 6, is designed for the redundant manipulator. When the redundant manipulator makes contact with a human at any position, there may be a positional deviation between the actual motion and the desired trajectory. To address this deviation, we utilize a mapping model that relates the stiffness to the end velocity of the manipulator. This model helps us determine changes in the manipulator's stiffness during operation, enabling the implementation of sliding mode variable impedance

control. Under the influence of the control force, the flexible contact dynamics equivalent twin system of the redundant manipulator is transformed into the joint acceleration component. We assess this component using joint angular acceleration as a criterion, optimizing joint velocity with the goal of minimizing cumulative deviations. Additionally, we convert the end motion component of the compliant process into the flexible motion component in the manipulator's joint space. By integrating manipulator motion planning with compliant motion generated by the collision, we achieve compliant control during human–robot multipoint contact interactions at any position.

### Design of multipoint contact compliance controller with variable parameters

The single-point contact force at any position can be estimated through the above section based on the Hertz theory and is equivalent to the force of the corresponding segment joint control point (equation (5)). Combined with the virtual end, it can be known that the estimated value of the force during multipoint contact is the accumulation of the estimated force of the segment joint where the contact point is located, that is:

$$f = \sum f_i (i = 1, 2, 3 \dots) \quad (13)$$

At this time, the position deviation generated when the manipulator has multipoint contact is represented by  $e$ , that is,  $e = x_d - x = x_d - g(q)$  as the error between the target and the current manipulator's end-pose. Where  $e = [e_x, e_y, e_z, e_{rx}, e_{ry}, e_{rz}]^T$  represents the translation error component and the rotation error component of the Rodrigues vector, the sliding surface  $s$  and the reaching law  $\dot{s}$  are set as follows:

$$e(t) = x_d(t) - x(t) \quad (14)$$

$$\dot{x}_r(t) = \dot{x}_d(t) + ce(t) \quad (15)$$

$$s(t) = \dot{x}_r(t) - \dot{x}(t) = \dot{e}(t) + ce(t) \quad (16)$$

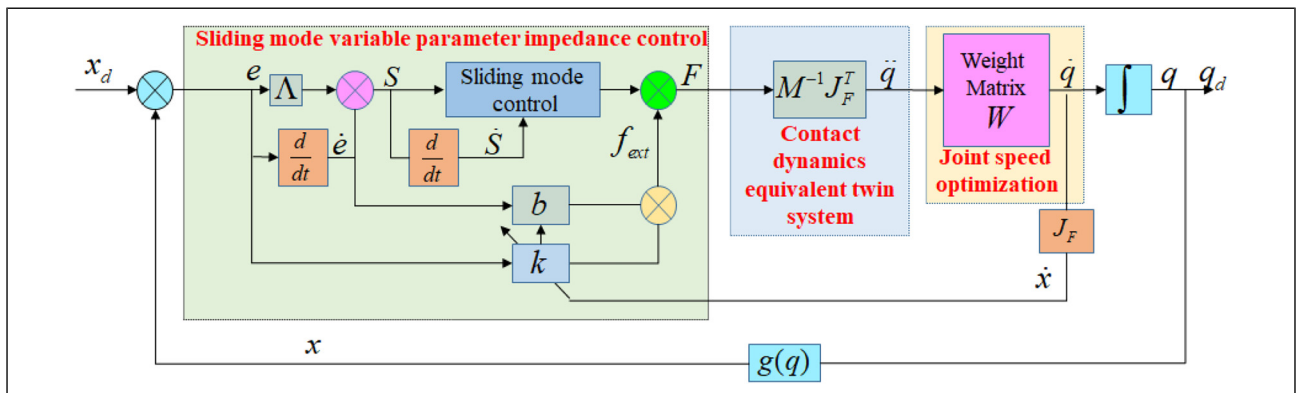


Figure 6. Block diagram of human–robot multipoint contact variable parameter compliance control strategy.

$$\dot{s}(t) = -\lambda s - \eta \tanh \frac{s}{\varepsilon} \quad (17)$$

Where  $e(t)$ ,  $s(t)$ ,  $\dot{s}(t)$  represent the position tracking error, the sliding surface, and the reaching law, respectively,  $c$  is a positive number that determines the rate of convergence of the sliding surface.  $\lambda$  and  $\eta$  both greater than zero,  $\|\Delta(q, \dot{q}, \ddot{q})\| \leq \eta$ .

Combined with the Cartesian space dynamics equation  $M_x(q)\ddot{x} + C_x(q, \dot{q})\dot{x} + G_x(q) = f - f_{ext}$  and impedance model expression  $m\ddot{x} + b\dot{x} + ke_x = f_{ext}$ , and substitute equation (16) into the impedance model to obtain:

$$f_{ext} = m\dot{s} - (mc - b + \frac{k}{c})\dot{e} + \frac{k}{c}s \quad (18)$$

Select the appropriate parameters so that:

$$mc - b + \frac{k}{c} = 0 \quad (19)$$

Substitute equations (14)–(16) into the kinetic equation to obtain:

$$(M_x - m)\dot{s} = M_x\dot{x}_r + C_x x_r + G_x(q) - C_x s + \frac{k}{c}s - f \quad (20)$$

Substituting equation (17) in equation (20), the equivalent twin system of the closed-loop dynamics based on the sliding mode impedance control can be obtained by the following equation:

$$(m\lambda + \frac{k}{c})s + \eta \tanh \frac{s}{\varepsilon} + f = 0 \quad (21)$$

It can be seen from equation (21) that only the controller parameters  $m$ ,  $\lambda$ ,  $k$ ,  $c$ ,  $\eta$ ,  $\varepsilon$  need to be adjusted, the compliance control of the manipulator under multipoint contact can be realized. Combining Equation (19) and stiffness  $k = b^2 / 4m\varepsilon^2$ , can be obtained:

$$b = 2mc \quad (22)$$

On the premise that the parameters  $m$ ,  $\varepsilon$  are selected as a definite value, the compliance control of the manipulator under multipoint contact at any position can be realized by adjusting the three parameters of  $\lambda$ ,  $k$ ,  $\eta$ . Among these three parameters, the stiffness matrix  $k$  directly affect the human–robot safety in the contact interaction task, the displacement of the end of the manipulator when it is subjected to external forces, that is, the soft or hard situation of the end movement, this parameter has a direct impact on the operation task. Therefore, the stiffness coefficient  $k$  is adjusted and controlled in real time during the movement of the manipulator in this paper.

### Setting of variable stiffness parameters

When the manipulator comes into contact with an object, the velocity of its end in Cartesian coordinates can change due to alterations in the contact force. To enhance the flexibility of operation, consider that the human arm

tends to exhibit greater stiffness in the primary direction of motion when subjected to external forces. This difference primarily stems from variations in speed components. Stiffness, being a nonnegative scalar, cannot undergo vector superposition in noncoordinate axis directions. Consequently, in this section, we configure the manipulator's stiffness parameter in two dimensions: the primary direction and the nonprimary direction of motion. This stiffness is oriented toward a changing ellipsoid, where the long axis aligns with the primary motion direction of the manipulator's virtual end velocity, while the short axis is set to one-fifth of the long axis. Suppose the relationship between compliance stiffness and velocity in the primary motion direction follows the following pattern:

$$k = k_0 + af(\dot{x}) \quad (23)$$

$$f(\dot{x}) = \frac{1}{1 - e^{-\dot{x}}} \quad (24)$$

Where  $k_0 \in R^6$  is the initial stiffness value, which can be given according to equation (2).  $a$  is a scalar representing the coefficient of variation of stiffness with velocity,  $\dot{x}$  is the real-time movement speed of the end of the manipulator,  $f(\cdot)$  is the mapping function between velocity and stiffness, which can be described by sigmoid function, i.e., equation (24). The change of the stiffness of the manipulator can be calculated in real time through the above equation.

### Joint angular velocity optimization under motion allocation of redundant degrees of freedom

When the manipulator experiences external contact forces, the variable parameter impedance control algorithm introduces additional motion to the original planned trajectory. This extra motion can gradually deviate the manipulator from its intended path. Left uncontrolled, this deviation can render the initial planning ineffective due to the accumulating error. For manipulators with redundant degrees of freedom, there are multiple solutions for joint angles derived from inverse kinematics, as well as numerous ways to allocate joint angular velocities to achieve the desired end-effector motion. In this section, we leverage the redundancy of the robot's degrees of freedom to compensate for motion deviations caused by the compliant motion component of the manipulator. This compensation ensures that the end velocity is distributed to the joint velocities while minimizing cumulative joint deviation.

The quadratic function that establishes the joint velocity is as follows:

$$V(\dot{q}) = \frac{1}{2}\dot{q}^T W \dot{q} \quad (25)$$

where  $\dot{q}$  is the joint speed,  $W \in R^{7 \times 7}$  represents the joint weight diagonal matrix, and each parameter on the diagonal represents the coefficient of each joint, namely  $W = \text{diag}(w_1, w_2, \dots, w_7)$ .

The selection of the diagonal element  $w_i$  of the weight matrix  $W$  can be judged and adjusted according to the joint angular acceleration of equation (10). That is,  $\ddot{q}_i > 0$ , indicating that it moves in the direction in which the motion component error generated by impedance control increases, and at this time, the weight needs to be increased to reduce the angular velocity; When  $\ddot{q}_i < 0$ , indicating that it moves in the direction of error reduction, and the weight should be reduced appropriately.

Here, the motion assignment weight transform element function is set to Sigmoid function, that is:

$$w_i(\ddot{q}_i) = \frac{e^{0.2\ddot{q}_i}}{1 + e^{0.2\ddot{q}_i}} \quad (26)$$

In order to find the minimum value of the quadratic form function in equation (25), the Lagrange multiplier method is used in combination with equation (7) to obtain the corrected quadratic form function as:

$$V(\dot{q}) = \frac{1}{2} \dot{q}^T W \dot{q} + \mu^T (\dot{x} - J \dot{q}) \quad (27)$$

Take the partial derivatives with respect to  $\dot{q}$  and  $\mu$  respectively:

$$\left(\frac{\partial V}{\partial \dot{q}}\right)^T = 0 \quad (28)$$

$$\left(\frac{\partial V}{\partial \mu}\right)^T = 0 \quad (29)$$

Based on equations (28) and (29), one can obtain:

$$\dot{q} = W^{-1} J^T \mu \quad (30)$$

Combined equations (7) and (30), we obtain:

$$\mu = (JW^{-1}J^T)^{-1}\dot{x} \quad (31)$$

Substituting  $\mu$  into equation (30), the minimum value function of the quadratic function is obtained:

$$\dot{q} = W^{-1}J^T(JW^{-1}J^T)^{-1}\dot{x} \quad (32)$$

To sum up, through the selection of the weight matrix  $W$ , the optimal distribution of the joint speed of the manipulator can be realized.

## Simulation analysis based on robot operating system platform

### Construction of virtual manipulator and simulation platform

Utilizing the system block diagram shown in Figure 6 and leveraging the robot operating system (ROS) platform along with Gazebo three-dimensional (3D) simulation software, we verified the effectiveness of the manipulator's compliance control method under multipoint contact through C++ programming. Given the complex mechanical structure and redundant degrees of freedom inherent in redundant manipulators, achieving precise geometric modeling can be challenging. Currently, most manipulator body structures can be modeled with the assistance of three-dimensional software, allowing us to obtain essential geometric parameters from these models. The specific modeling process is illustrated in Figure 7. It involves creating

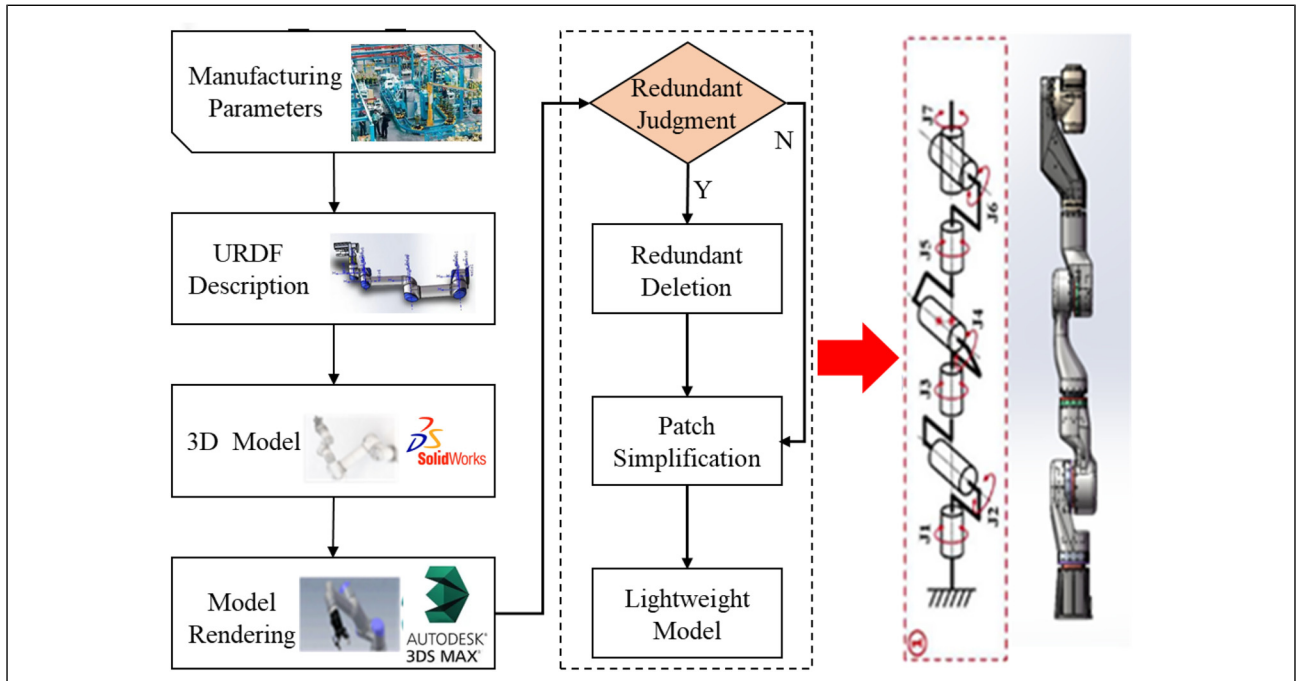


**Figure 7.** Flow chart of geometric modeling of manipulator.

a unified robot description format model based on the D-H parameter. We define the links, joints, and their relationships while also configuring the colors, materials, and gravity of the links. Additionally, we manage the transmission and control of the joints using plugins such as “gazebo\_ROS\_control.”

The implementation process of human–robot multipoint contact compliance control is depicted in Figure 8. The manipulator system comprises various components, including manipulator hardware, hardware interface, joint controller, controller manager, compliance controller, joint state publisher, robot state publisher, and motion planner. The manipulator hardware interacts with the hardware interface node through read and write operations. In the compliance control system, the controller manager oversees both the joint controller and the compliance controller (the compliance control algorithm proposed here is packaged as a

plug-in). It manages the loading and closing of these controllers. Following the control strategy outlined in this paper, the required joint angular acceleration for compliance control is calculated. The joint angular velocity and joint angle are then determined by multiplying the control period and are subsequently passed to the motion planner. The system operates at a control frequency of 50 Hz. The motion planner (MoveIt!) subscribes to the robot pose issued by the hardware interface, which has been processed by the joint state publisher and the robot state publisher. The motion planner then plans an appropriate motion trajectory, taking into account the target state issued by the compliance controller, and delivers this trajectory to the joint controller. The joint controller, in turn, issues the joint speeds to the hardware interface to control the motion of the manipulator. This cycle repeats to accomplish the compliance control of the manipulator.

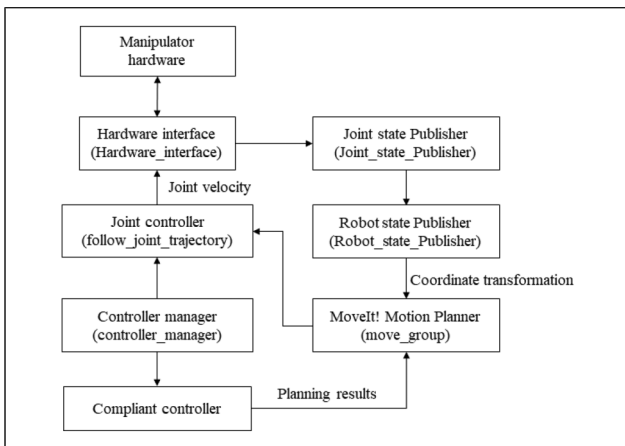


**Figure 8.** Flow chart of human–robot multipoint contact compliance control.

### Analysis of simulation results

By packaging the algorithm in the above section, the simulation of multipoint contact compliance control of redundant manipulator is carried out on the ROS system platform combined with Gazebo 3D simulation software. Figure 9 shows the motion of the redundant manipulator under the action of external contact force when a contact force in the  $x$ -direction is applied to the upper arm of the manipulator (represented by Link2) at a distance of 0.1 m from the shoulder joint in a static state, and the magnitude is 6 N.

To verify the effectiveness of the theoretical algorithm, we begin with a static state where the manipulator arm Link2 is not controlled, and impedance control is applied at any point of contact, as shown in Figure 10. Figure 10(a) and (b) displays the force and joint angle values on the control nodes of the manipulator skeleton

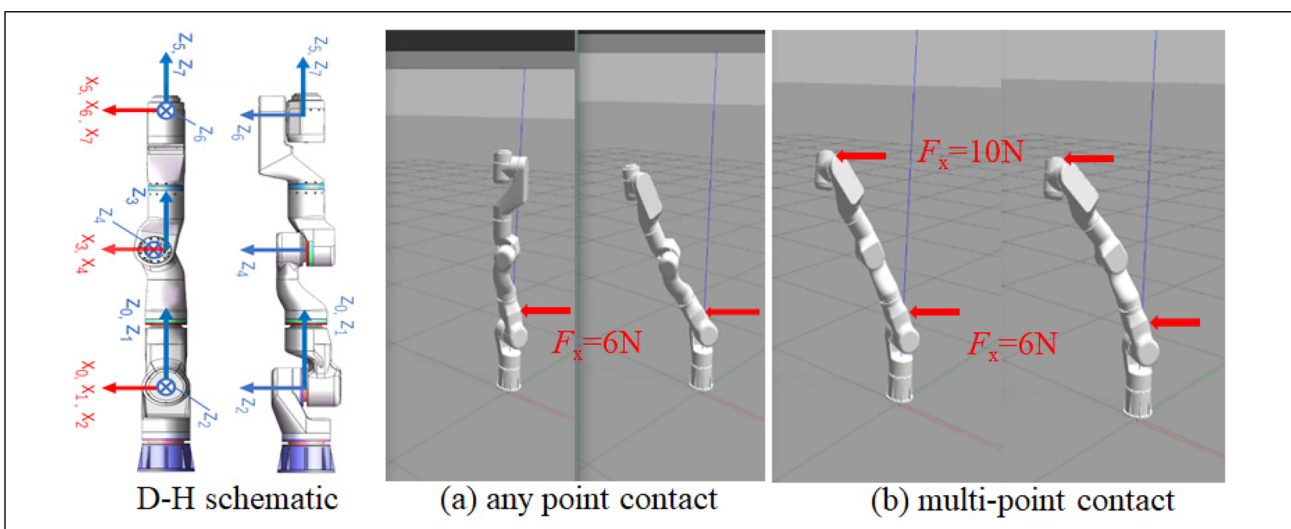


**Figure 9.** Motion simulation diagram of redundant manipulator under static contact at any point and multipoint contact.

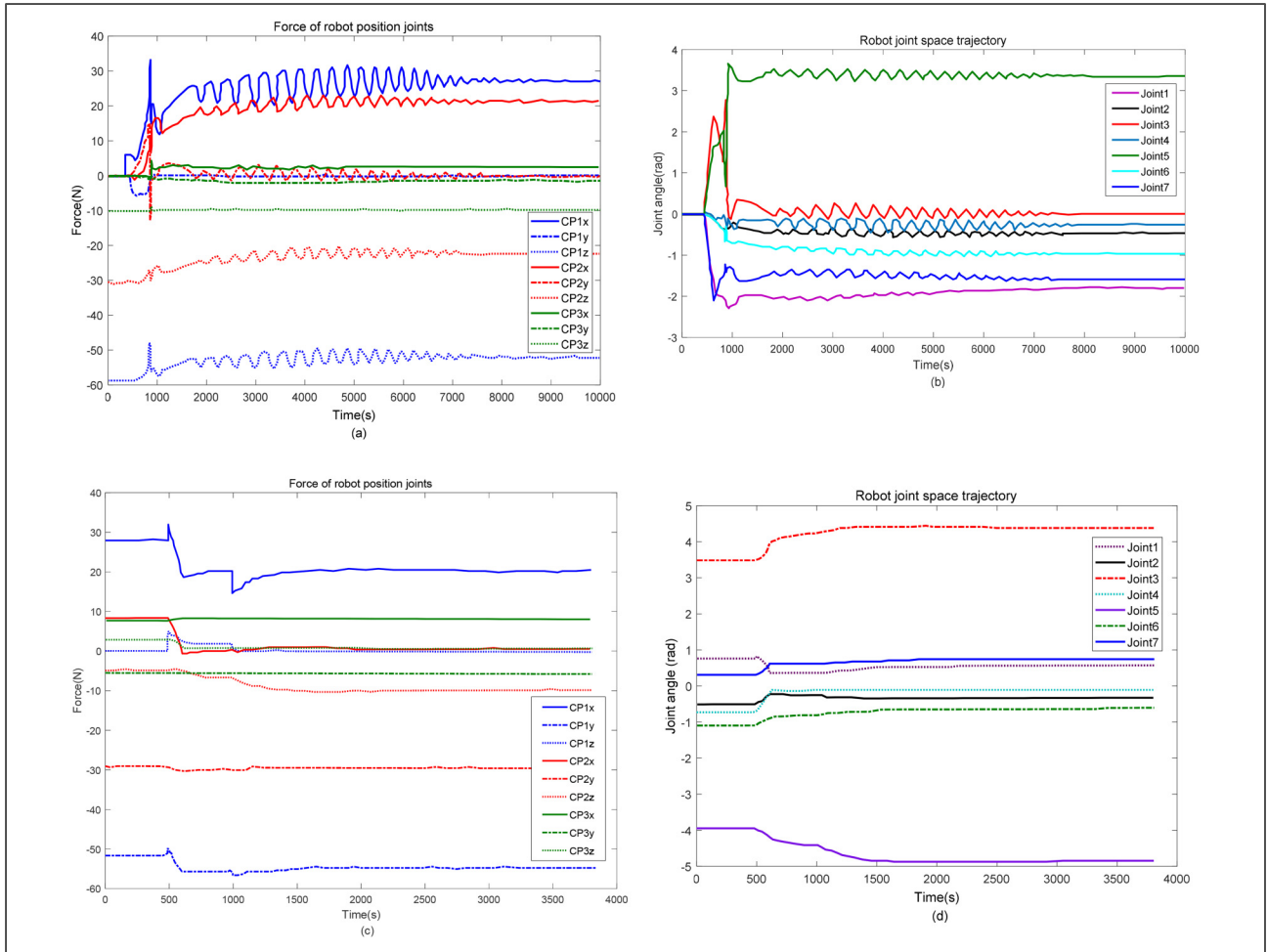


**Figure 10.** Simulation results of any point contact of the upper arm of the redundant manipulator.

when the control algorithm is not applied under the influence of external contact force. In contrast, Figure 10(c) and (d) shows the force and joint angle values on the three control nodes of the manipulator when using the compliance control algorithm proposed in this paper under external force. Notably, in Figure 10, the  $y$ -direction force values of the three control nodes also include the gravity values of the segmented links where the manipulator is positioned, as per the conversion relationship between each joint and the tool coordinate system.

It can be seen from Figure 10(a) and (c) that for the two endpoints of the segment where the contact position of the manipulator is located in the human–robot contact interaction, the control point  $CP_1$  at the end close to the applied force receives a greater force, while the control point  $CP_3$  of the skeleton segment far away from the contact point almost has no effect. The method of multiple virtual ends based on the skeleton is feasible from the point of view of the force on the control node of the manipulator skeleton when the human–robot interaction contacts any point. By analyzing Figure 10(a) and (b), it can be seen that the manipulator appears buffeting and instability

without compliance compensation, and the force transferred to the control joint is large, which is not conducive to the safety of the human/manipulator and may cause damage to the manipulator body. Figure 10(c) and (d) is the result of applying the compliance control algorithm in this paper. It can be seen that during the duration of the manipulator force, the force changes on the two control nodes  $CP_1$  and  $CP_2$  of the segmented upper arm where the manipulator force is applied, and  $CP_3$  almost does not change. Because the contact force is in the  $x$ -direction, the force change in the  $x$ -direction of the closer  $CP_1$  node is relatively large, but not more than 10 N, which is much smaller and more stable than that in Figure 10(a) without compliance control. At this time, the manipulator moves smoothly, and the corresponding joint angle changes smoothly.

On the basis of applying a 6N contact force in the  $x$ -direction at the position where the upper arm is 0.1 m away from the shoulder joint in Figure 9, a 10 N force in the  $x$ -direction is applied at the end of the manipulator at the same time to simulate the multipoint contact between human and robot. Figure 11 shows the multipoint contact simulation results of the redundant manipulator with static

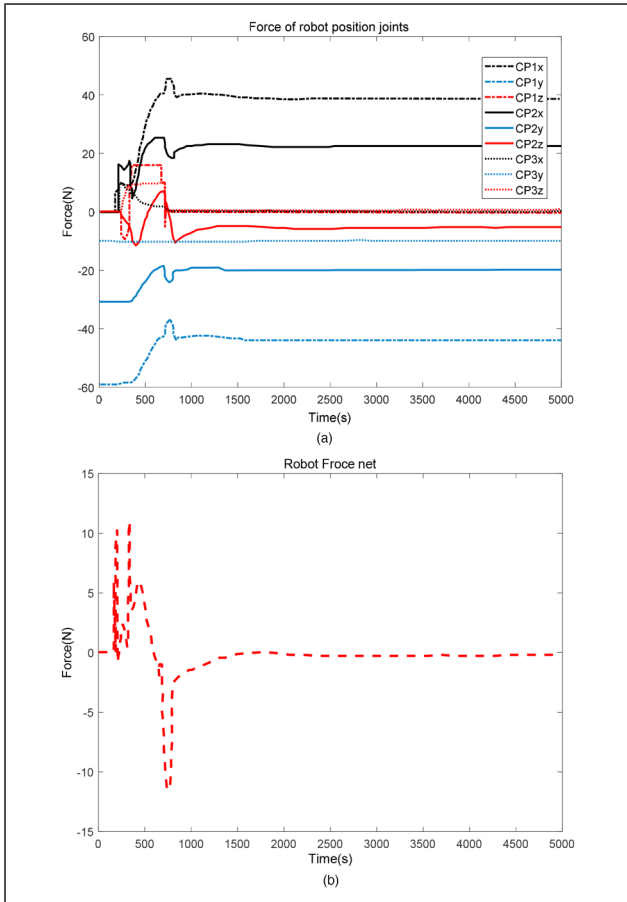


**Figure 11.** Simulation results of multipoint contact of human-robot static interaction redundant manipulator.

human-robot interaction. As can be seen from Figure 11(a), a force change occurs at the control point  $CP_3$  under the multipoint contact, and the force is transmitted from the force point toward the base, so that the force change is the largest at the control point  $CP_1$ . Under the action of the compliance control algorithm, the change range of the whole force is within 10 N, and it is relatively stable, so the manipulator joints move smoothly and slowly when the human-robot contacts at multiple points (Figure 11(b)).

In addition, when the manipulator moves from the initial state to the end point (0.6, 0.5, 0.5) m in Cartesian coordinates, the joint angles of the manipulator can be obtained by inverse kinematics, so the motion planning in Cartesian space can be transformed into joint space, and the desired joint angles of the manipulator can be obtained. When the redundant manipulator is subjected to a contact force of 6 N in the  $x$ -direction at a distance of 0.1 m from the shoulder joint of the upper arm of the manipulator in the process of motion planning, as shown in Figure 12(a), the end of the manipulator deviates from the established trajectory within a short period of time (1200–3000 s) of contact. Under the action of the flexible contact dynamics system and the compliance control strategy, the maximum offset

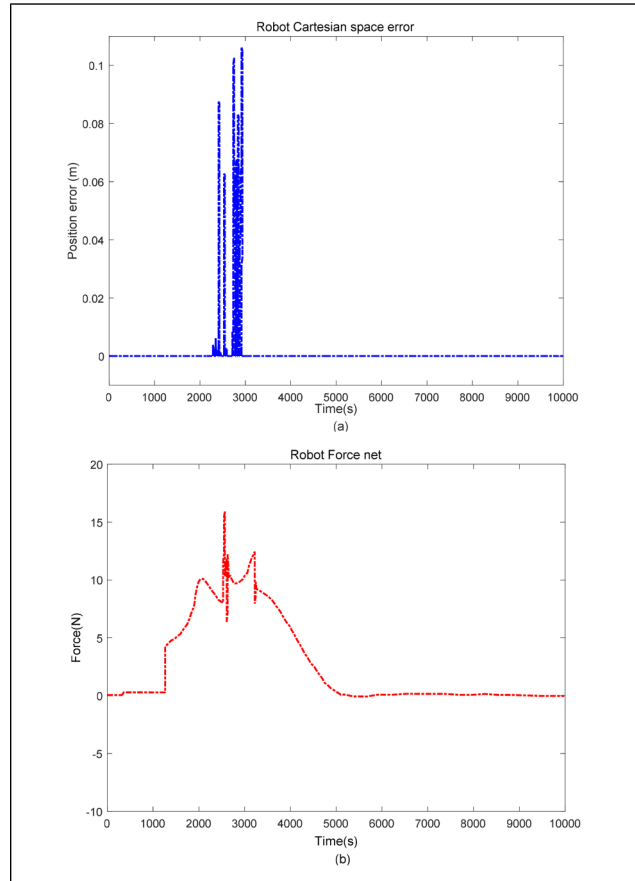


**Figure 12.** Simulation result of contact at any point during movement of redundant manipulator.

is not at the moment of just contact, and the maximum deviation is controlled at about 0.1 m due to a certain buffer and compliance effect. In the process of movement, the force variation range under the contact action of any position of the manipulator is within 15 N, which is relatively stable and gradually returns to 0 N, which can ensure the safety of contact interaction between the manipulator and human in the process of movement (Figure 12(b)).

On the basis of the implementation conditions in Figure 12, in addition to the 6 N contact force in the  $x$ -direction at 0.1 m from the shoulder joint of the upper arm of manipulator, 10 N contact force in the  $x$ -direction at the end of the manipulator is added to simulate the human-robot multipoint contact during the movement, the simulation results are shown in Figure 13. It can be seen from Figure 13(a)–(b) that the multipoint contact force is applied on the basis of the original motion, and the sudden change of the two forces and the superposition effect of the forces obviously appear on the graph. Under the action of the compliance control strategy in this paper, the multipoint contact during the motion of the manipulator can also ensure the smooth motion trajectory of the joint. The

maximum error at the end of the manipulator is 0.6 m and gradually decreases to about zero, returning to the expected motion (Figure 13(c)–(d)).

the manipulator will undergo displacement. The end velocity of the segment with the most significant displacement component is used as the velocity in the main motion direction to adapt the manipulator’s stiffness coefficient.

### Experimental verification of multipoint variable parameter compliance control

To validate the implementation effectiveness of the multipoint contact resultant force calculation method proposed in this paper on the control system, multipoint contact experiments involving different link segments are conducted in this section. By applying pressure simultaneously at various positions on different links using hands, the manipulator responds to the magnitude and direction of the resultant force. The experiment is depicted in Figure 14.

Adjusting the manipulator’s stiffness based on the intended human–robot interaction is a key element in achieving compliance control for safe human–robot interactions. Similarly, when both the upper arm and lower arm of the manipulator experience contact forces, each segment of



Figure 14. Human–robot interaction multipoint contact experiment diagram.

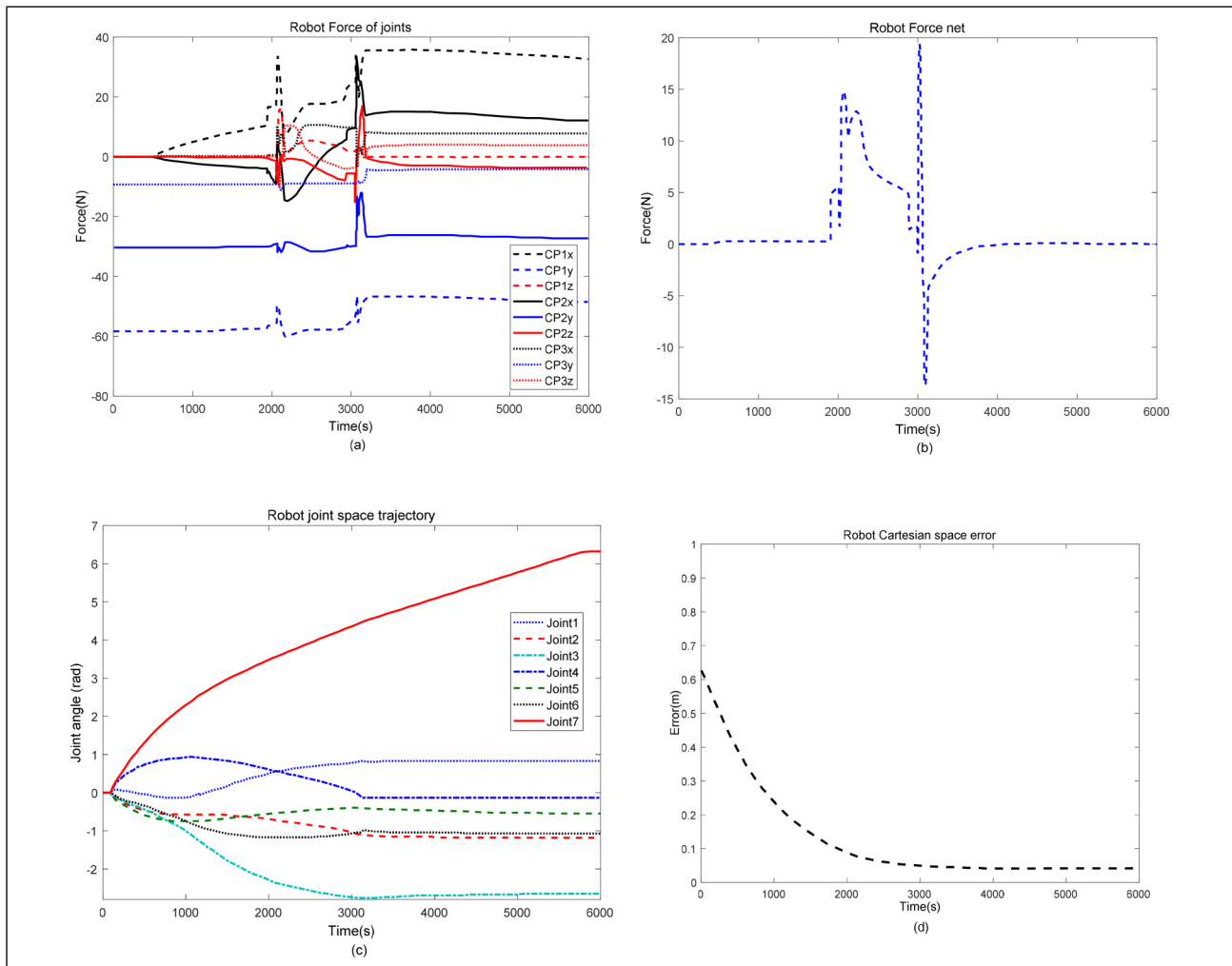
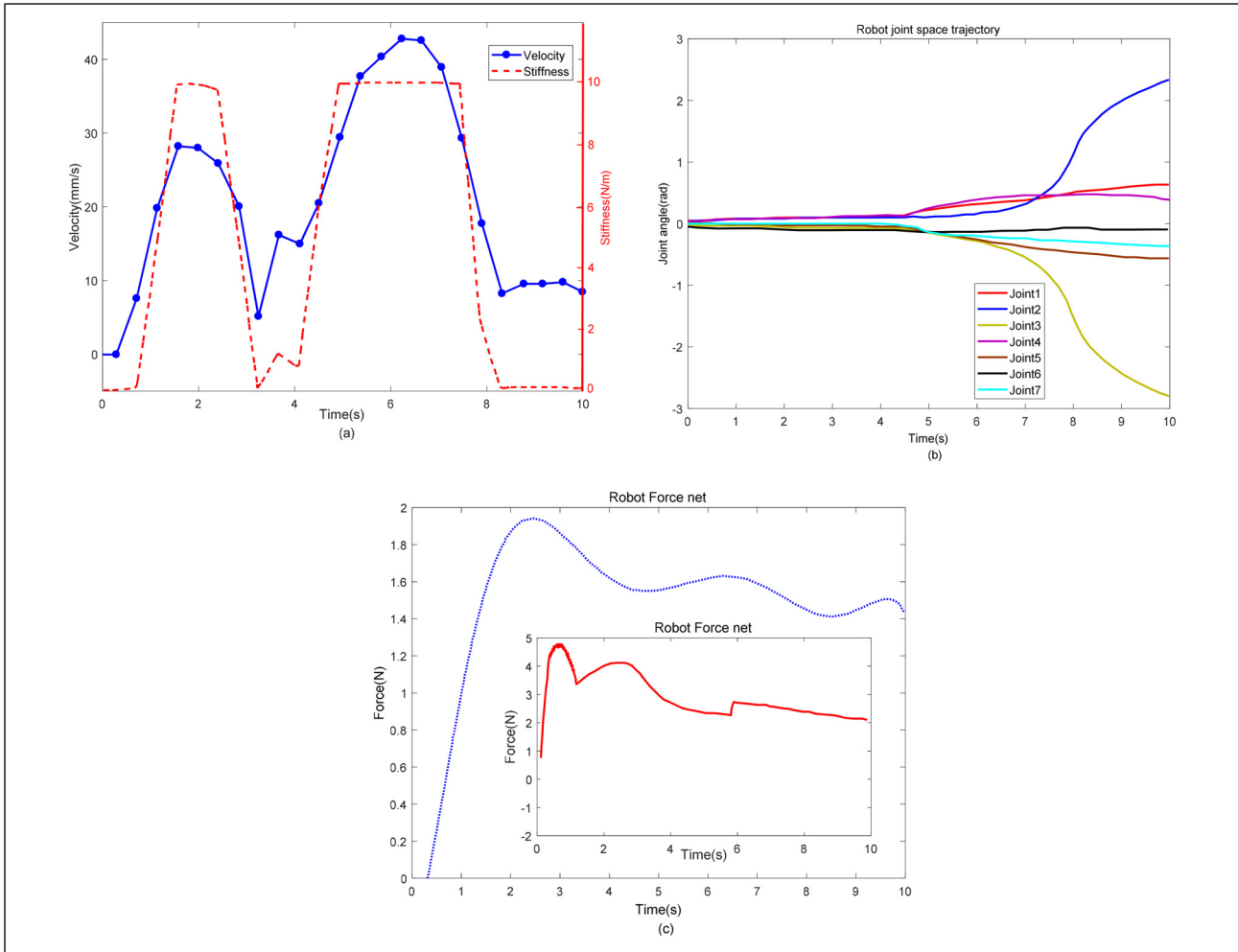


Figure 13. Simulation results of multipoint contact during movement of redundant manipulator.



**Figure 15.** Human–robot interaction multipoint contact experiment result. (a) Variable stiffness coefficient setting (b) angle change of each joint of the manipulator (c) contact force resultant with or without compliance control.

Figure 15(a) illustrates the setup for impedance control parameter stiffness coefficient under human–robot multipoint contact. In the figure, the blue dotted and solid lines represent the velocity of the virtual end of the multipoint contact segment of the manipulator in the main motion direction, while the red dotted line represents the stiffness coefficient calculated according to the method proposed in this paper. It's evident from the figure that as the manipulator comes into contact with a human, different stiffness values are selected to ensure compliance, adjusting in response to changes in the main motion direction's speed.

Figure 15(b) is the movement change diagram of each joint angle of the manipulator under the multi-point contact between the human and the robot. In the process of multipoint contact at any position, the change of the joint angle of the manipulator is stable, and the angles of the corresponding joints 2 and 3 of the upper arm and the lower arm where the contact points are located change greatly, but there is no stutter or mutation. In the first 5 s, because the speed of the segmented main motion generated by the force changes slightly, it can be seen that the joints of

the manipulator change slowly at this time. After 5 s, with the increase of the speed, the corresponding offset of the manipulator increases, and the angular velocity of each joint of the manipulator changes greatly, so it can be seen that the angle of each joint of the manipulator changes greatly after 5 s.

Figure 15(c) presents a comparison of the resultant force curves between cases without compliance control and with the compliance control algorithm proposed in this paper over the corresponding time frame. The embedded graph displays the contact force under multipoint contact calculated without the control algorithm, which eventually stabilizes at approximately 2.5 N. In contrast, when applying the compliance control algorithm proposed in this paper, the contact force stabilizes at around 1.5 N, which represents 60% of the contact force observed without control. This demonstrates that the flexible contact dynamics equivalent twin system and control method can effectively reduce contact force while maintaining compliant motion of the manipulator in multipoint contact scenarios during human–robot interaction.

## Conclusion

In this study, we propose the VEER arbitrary point contact dynamic model to elucidate the dynamic coupling mechanism in the human–robot interaction of redundant manipulators within confined spaces. This model facilitates the conversion of contact forces by integrating with the skeleton principle. We construct a flexible contact dynamic equivalent twin system for redundant manipulators engaged in multipoint or arbitrary point contact scenarios. Leveraging the redundancy in the degree of freedom motion, we achieve optimal joint speed distribution by minimizing cumulative joint deviations. Furthermore, we adjust the impedance stiffness coefficient in real-time based on the manipulator’s end-effector velocity to enable variable parameter compliance control during multipoint contact interactions for human–robot safety. To validate our approach, we employ the ROS system for simulation, analyzing the multipoint contact dynamic model of redundant manipulators and assessing the feasibility of our variable parameter compliance control method. The effectiveness and practicality of our proposed compliance control method are confirmed through simulation and experimental results.

This research offers a novel perspective for achieving human–robot multipoint contact interactions within complex and dynamic confined environments. However, the actual human–robot interaction is in large physical contact with the redundant manipulators, so the flexible contact dynamics model still needs to be further improved; meanwhile, multipoint human–robot interaction in highly dynamic environments is still a major challenge.

## Data Availability Statement

The data are available from the corresponding author on reasonable request.

## Declaration of conflicting interests

The authors declared no potential conflicts of interest with respect to the research, authorship, and/or publication of this article.

## Funding

The authors disclosed receipt of the following financial support for the research, authorship, and/or publication of this article: This work was supported by the Capacity Building Plan for local colleges and universities of Shanghai Scientific Committee, National Natural Science Foundation of China, and National Key Research and Development Program of China (Grant Nos. 23010501600, 61263045, 61763030, and 2018YFB1305300).

## ORCID iD

Xiaoqing Zhang  <https://orcid.org/0009-0004-1931-9932>

## References

- Atawnih A, Papageorgiou D and Doulgeri Z. Kinematic control of redundant robots with guaranteed joint limit avoidance. *Robotics and Autonomous Systems* 2016; 79: 122–131.
- Simas H and Di Gregorio R. Smooth transition for collision avoidance of redundant robots: an on-line polynomial approach. *Robotics and Computer-Integrated Manufacturing* 2021; 72: 102087.
- Zhang Z, Zheng L, Chen Z, et al. Mutual-collision-avoidance scheme synthesized by neural networks for dual redundant robot manipulators executing cooperative tasks. *IEEE Transactions on Neural Networks and Learning Systems* 2021; 32: 1052–1066.
- Chen YJ, Ju MY and Hwang KS. A virtual torque-based approach to kinematic control of redundant manipulators. *IEEE Transactions on Industrial Electronics* 2017; 64: 1728–1736.
- Pan Y, Du P, Xue H, et al. Singularity-free fixed-time fuzzy control for robotic systems with user-defined performance. *IEEE Transactions on Fuzzy Systems* 2021; 29: 2388–2398.
- Lee D, Lee W, Park J, et al. Task space control of articulated robot near kinematic singularity: forward dynamics approach. *IEEE Robotics and Automation Letters* 2020; 5: 752–759.
- Kemp C, Edsinger A and Torres-Jara E. Challenges for robot manipulation in human environments [grand challenges of robotics]. *Robotics & Automation Magazine IEEE* 2007; 14: 20–29.
- Hogan N. Impedance control: an approach to manipulation. *J Dyn Syst Meas Contr* 1985; 107: 8–16.
- Kazerouni H, Sheridan TB and Houpt PK. Robust compliant motion for manipulators, part I: the fundamental concepts of compliant motion. *IEEE Journal on Robotics and Automation* 1986; 2: 83–92.
- Zeng G and Hemami A. An overview of robot force control. *Robotica* 1997; 15: 473–482.
- Zhang H and Paul R. Hybrid control of robot manipulators. *IEEE International Conference on Robotics and Automation* 1985; 2: 602–607.
- Song G and Cai L. Robust position/force control of robot manipulators during constrained tasks. *IEEE Proceedings-Control Theory and Applications* 1998; 145: 427–433.
- Dong B, An T, Zhou F, et al. Model-free optimal decentralized sliding mode control for modular and re-configurable robots based on adaptive dynamic programming. *Adv Mech Eng* 2019; 11: 168781401989692.
- Wang F, Chao Z, Huang L, et al. Trajectory tracking control of robot manipulator based on RBF neural network and fuzzy sliding mode. *Cluster Comput* 2019; 22: 5799–5809.
- Xiang GD, Yu XD and Li CD. Robust adaptive position/force hybrid control for constrained robotic manipulators. *Journal of System Simulation* 2007; 19: 348–351.
- Hogan N. Impedance control: an approach to manipulation. Part I: theory; part II: implementation; part III: application. *Journal of Dynamic Systems Measurement and Control-Transactions of the ASME* 1985; 107: 304–313.
- Ott C, Mukherjee R and Nakamura Y. Unified impedance and admittance control. In: *Proceedings IEEE international conference on robotics and automation*, Anchorage, AK, USA, 2010, pp.554–561IEEE.
- Mao D, Yang W and Du Z. Fuzzy variable impedance control based on stiffness identification for human-robot cooperation. *IOP Conf Ser Earth Environ Sci* 2017; 69: 012090.

19. Seraji H and Colbaugh R. Force tracking in impedance control. *International Journal of Robotics Research* 1993; 16: 97–117.
20. Lu W S and Meng Q H. Impedance control with adaptation for robotic manipulations. *IEEE Transactions on Robotics and Automation* 1991; 7: 408–415.
21. Ikeura R, Moriguchi T and Mizutani K. Optimal variable impedance control for a robot and its application to lifting an object with a human. In: *Proceedings 11th IEEE international workshop on robot and human interactive communication*, Berlin, Germany, 2002, pp.500–505. IEEE.
22. Tsumugiwa T, Yokogawa R and Hara K. Variable impedance control based on estimation of human arm stiffness for human-robot cooperative calligraphic task. In: *Proceedings 2002 IEEE international conference on robotics and automation (cat. No. 02CH37292)*, Washington, DC, USA, 2002, pp.644–650. IEEE.
23. Sharifi M, Behzadipour S and Vossoughi GR. Model reference adaptive impedance control in Cartesian coordinates for physical human-robot interaction. *Adv Robotics* 2014; 28: 1277–1290.
24. Peng ZX and Adachi N. Compliant motion control of kinematically redundant manipulators. *IEEE Transactions on Robotics & Automation* 1991; 9: 831–836.
25. Ficuciello F, Villani L and Siciliano B. Variable impedance control of redundant manipulators for intuitive human-robot physical interaction. *IEEE Trans. Rob* 2015; 31: 850–863.
26. Xiong G L, Chen H C, Xiong P W, et al. Cartesian impedance control for physical human-robot interaction using virtual decomposition control approach. *Iran J Sci Technol Trans Mech Eng* 2018; 43: 983–994.
27. Li Y, Ganesh G, Jarrasse N, et al. Force, impedance, and trajectory learning for contact tooling and haptic identification. *IEEE Trans. Robot* 2018; 34: 1170–1182.
28. Peng ZX and Adachi N. Compliant motion control of kinematically redundant manipulators. *IEEE Transactions on Robotics and Automation* 1993; 9: 831–836.
29. Hua L, Zhang FH and Fu YL. An impedance control method of 7-DOF redundant manipulator. *Journal of Huazhong University of Science and Technology (Natural Science)* 2013, 41: 42–46.
30. Lin ZC, Patel RV and Balafoutis CA. Impact reduction for redundant manipulators using augmented impedance control. *Journal of Robotic Systems* 1995; 12: 301–313.
31. Zhao J, Lv Y, Zeng Q, et al. Online policy learning based output-feedback optimal control of continuous-time systems. *IEEE Transactions on Circuits and Systems II: Express Briefs* 2022; 71: 652–656.
32. Qi W, Ovrur S E, Li Z, et al. Multi-sensor guided hand gesture recognition for a teleoperated robot using a recurrent neural network. *IEEE Robotics and Automation Letters* 2021; 6: 6039–6045.
33. Gonthier Y. Contact dynamics modelling for robotic task simulation. PhD Thesis, 2007, pp.15–32.
34. Hunt KH and Crossley FR. Coefficient of restitution interpreted as damping in vibroimpact. *Transactions of the ASME Journal of Applied Mechanics, Series E* 1975; 42: 440–445.
35. Ye L, Xiong G, Zhang H, et al. Sensor-based skeleton modeling and MVEEs approach of the redundant manipulator for reaction motion. *Advances in Mechanical Engineering* 2022; 14: 168781402210742.
36. Seto F, Kosuge K and Hirata Y. Real-time self-collision avoidance system for robots using ROBE. *International Journal of Humanoid Robotics* 2004; 01: 533–550.